Solar Photocatalytic Oxidation of As^{3+} in Aqueous Solution by $TiO_2/SrCO_3$ and $Ag.TiO_2/SrCO_3$ Composite Photocatalysts

Pakpoom Hanpee[1*], Jukkriwut Morkarn[2], Oranooch Somseemee[2] and Wichien Sang-aroon[2]

[1] Regional Medical Sciences Center 7 Khon Kaen, 349 Moo 19, Siharat Dechochai Road, Sila, Muang Khon Kaen, Khon Kaen, 40000

[2] Department of Chemistry, Faculty of Engineering, Rajamagala University of Technology Isan, Khon Kaen campus, 150 Moo 6, Srichan Road, Muang Khon Kaen, Khon Kaen, 40000

*Corresponding Author: pakpoomkem@gmail.com

Received 14 December 2024; Received in revised form 27 December 2024; Accepted 28 December 2024

Abstract

This work has observed and reported solar photocatalytic oxidation of As^{3+} in an aqueous solution by $Ag\text{-}SrTiO_3$. The effect of pH, catalyst loading, initial concentration of As^{3+}, and sacrificial reagent was investigated. The thermodynamics and kinetics of conversion of As^{3+} to As^{5+} were determined by the change in As^{3+} concentration by utilizing UV-Vis spectrophotometry as a function of irradiation time. The observed kinetics of photocatalytic oxidation of As^{3+} follows a pseudo-first-order kinetic model. The results showed a significant dependence of the photocatalytic oxidation of As^{3+} on the functional parameters.

Keywords: Photocatalytic oxidation; As^{3+}; Advance oxidation process; $Ag\text{-}SrTiO_3$; Solar light

1. Introduction

Arsenic is one of the most toxic and carcinogenic elements [1] and is occupied in the VA group in the periodic table. The most common oxidation state is trivalent (As^{3+}) but less in the pentavalent (As^{5+}) state. As^{3+} is presented in the form of both organic and inorganic species in natural water. The species of inorganic arsenic are dependent on the redox conditions and the pH. It is known that As^{3+} is high and more toxic than those As^{5+}. Many countries have geological environments conducive to the generation of high-arsenic groundwater [2]. Wild-spread contamination of arsenic in groundwater has led to a massive epidemic of arsenic poisoning. Based on the World Health Organization; WHO's standards, arsenic concentrations have to be under 10 ppb but it is estimated that more than 57 million people from around the world are drinking arsenic-contaminated groundwater above that standard concentration [3]. Therefore, it is important to find new methods or technology to access this regulation. A large number of technologies have been tested for the removal of arsenic from groundwater [4]. The methods include coagulation and precipitation [5], membrane separation [4], ion exchange [6], and adsorption [7].

However, these methods also contain a waste stream of As^{3+} and need further methods to oxidize As^{3+} to As^{5+} before release to the environment. According to the slow rate of oxidation by oxygen, more oxidizing species such as chlorine, ozone, or permanganate are needed. Unfortunately, the use of those oxidizing species may cause toxic species by-products, for example, the use of chlorine can generate organochlorine compounds which are toxic substances.

In recent areas, advanced oxidation processes (AOPs) have been found as an effective and alternative way for the treatment of organic and inorganic substances. AOPs result in the generation of hydroxyl radicals (OH•) as main oxidizing agents which can remove even nonbiodegradable organic and inorganic compounds from the wastewater stream. The AOPs based on photocatalysts are valuable in completely degrading organic pollutants to CO_2 and H_2O. Similarly, photocatalysts have easily converted the inorganic pollutant from highly toxic species to less toxic species. The best methodology for the treatment of toxic organic and inorganic effluents is using the oxide of semiconductors as photocatalyst such as TiO_2, ZnO, ZnS, WO, CdS, Fe_2O_3, and $SrTiO_3$ [8-13]. Among them, TiO_2 has been widely applied as a photocatalyst due to its high activity, nontoxicity, chemical stability, lower costs, optical and electrical properties, and environment-friendly characteristics.

Photocatalytic activity of TiO_2 can be improved by doping metal and/or forming composite with other materials. $SrCO_3$ can be used as a composite for the oxide of semiconductors in the field of photocatalysis based on its high adsorption ability. So, in this work, solar photocatalytic oxidation of As^{3+} in aqueous solution by $TiO_2/SrCO_3$ and $Ag\text{-}TiO_2/SrCO_3$ has been reported. The effects of parameters such as pH, catalyst loading, and initial concentration of As^{3+} were investigated. The kinetic conversion of As^{3+} to As^{5+} was determined by the change in As^{3+} concentration by employing a UV-Vis spectrophotometer as a function of irradiation time. The thermodynamic quantities of the photocatalytic reaction were also determined and reported.

2. Experimental

2.1 Overview of photocatalytic oxidation

The photocatalytic oxidation of $SrTiO_3$ and $Ag.SrTiO_3$ is described in Fig. 1. The photocatalytic process occurs with 3 main steps including:

1) Charge separation step; a step in which photocatalyst absorbs photon then electrons from the valence band are excited to conduction band forming an electron-hole as eq. 1 separation:

$$SrTiO_3/Ag.SrTiO_3 + h\nu \longrightarrow SrTiO_3/Ag.SrTiO_3 (e^- + h^+) \quad (1)$$

2) Radical formation; The important step that strong oxidizing species such as $OH^{\bullet}$, $H^{\bullet}$ and $O_2^{\bullet -}$ are formed via equation (2)-(8)

$$h^+ + OH^- \longrightarrow OH^{\bullet} \quad (2)$$

$$h^+ + H_2O \longrightarrow OH^{\bullet} + H^+ \quad (3)$$

$$e^- + O_2 \longrightarrow O_2^{\bullet -} \quad (4)$$

$$H^+ + O^{\bullet} \longrightarrow OH^{\bullet} \quad (5)$$

$2H_2O + O_2^{\bullet -} \longrightarrow 2H_2O_2$ (6)

$H_2O_2 \longrightarrow 2OH^{\bullet}$ (7)

$H^+ + e^- \longrightarrow H^{\bullet}$ (8)

when

h^+ is valence band hole

e^- is conduction electron)

$OH^{\bullet}$ is hydroxyl radical

$O_2^{\bullet -}$ is superoxide ion radical

$OH_2^{\bullet}$ is perhydroxyl radical

$H^{\bullet}$ is hydrogen radical

3) Electron-hole recombination; conduction band electron can be recombined with a valence hole as equation:

$e^- + h^+ \longrightarrow$ Heat (9)

$OH^{\bullet}$, $O_2^{\bullet -}$, $OH_2^{\bullet}$, and $H^{\bullet}$ are strong oxidizing species that can be formed by both valence hole and conduction band electrons.

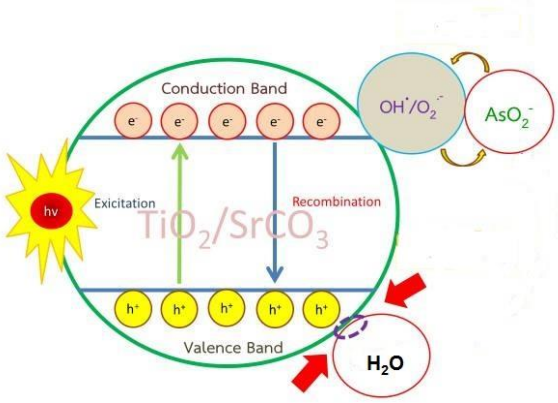

Figure 1 Schematic representation of photocatalytic oxidation of arsenic by $TiO_2/SrCO_3$

2.2 Synthesis of $TiO_2/SrCO_3$ and $Ag.TiO_2/SrCO_3$

The composite $TiO_2/SrCO_3$ powders were synthesized by sol-gel method by using TiO_2 and $SrCO_3$ as starting materials. The amount of starting materials was calculated with a 1:1 mole ratio. The two materials were mixed well in HCl solution pH 1. The slurry was stirred well and then dried in the air oven at 100 °C for 12 hrs. The dried solid was grounded in an agate mortar and then calcined at 600 °C for 6 hrs in a furnace.

The photocatalysts; $Ag.TiO_2/SrCO_3$ was synthesized by the photodeposition method. 2 g of obtained $TiO_2/SrCO_3$ was dissolved in 50 mL of deionized water. The solution was adjusted to pH 1 by HCl solution. The amount of $AgNO_3$ (QReC Co, Ltd) with a 1-mole ratio versus $SrTiO_3$ was required to be added into a slurry. The slurry was stirred well under UV irradiation for 3 hrs and then dried in the air oven at 100 °C for 12 hrs. The dried solid was grounded in an agate mortar and then calcined at 600 °C for 6 hrs in a furnace.

2.3 Photocatalytic determination

Photocatalytic activity of $TiO_2/SrCO_3$ and $Ag.TiO_2/SrCO_3$ were performed by the batch technique. The parameters affecting the photocatalytic efficiency of the photocatalysts were studied including initial concentration of As^{3+}, amount of photocatalyst, pH of solution, and temperature. Each photocatalytic experiment was performed in a 500 mL beaker. During the experiment, the test solution in the beaker was constantly stirred and illuminated by the sun. One gram of photocatalyst was added into 250 mL of $NaAsO_2$ (QRec Co, Ltd) solution sample. Concentrations of $NaAsO_2$ solution were 0.5, 1, 5, 10 and 50 ppm. Each experiment was run within 1 hour. All experiments were carried out at ambient temperature. The radiation density flux on the reactor was determined by a light meter for each run.

2.4 Determination of As^{3+} concentration

The oxidizing species can oxidize As^{3+} O_2^- to $H_2AsO_4^-$ as in equation:

$$AsO_2^- \xrightarrow{OH^\bullet / O_2^{\bullet -}} H_2AsO_4 \qquad (10)$$

The concentration of residual As^{3+} in the solution at various times was determined colorimetric method. The method employs oxidation of $H_2AsO_4^-$ by I^- then I_2 (eq. 2) which is a product of the reaction was reduced by rhodamine B. The disappearance of rhodamine B is related to the concentration of As^{3+} (eq. 3). The absorbance of rhodamine B was determined at 543 nm by UV-Vis spectrophotometer (T80+ model UV-Vis spectrophotometer, PG Instrument Ltd)

$$H_2AsO_4^- + 2H^+ + 2I^- \rightarrow H_2AsO_3^- + H_2O + I_2 \qquad (11)$$

$$I_2 + RhB(colored) \rightarrow 2I^- + RhB(colorless) \qquad (12)$$

2.5 Photocatalytic oxidation efficiency

The efficiency is calculated based on the equation:

$$\%efficiency = \frac{C_0 - C_t}{C_t} x100 \qquad (13)$$

where C_0 and C_t are initial and variable concentrations of As^{3+}, respectively.

2.6 Photocatalytic oxidation kinetics

The kinetics of the photocatalytic oxidation of As^{3+} by the photocatalysts was analyzed in terms of pseudo first- and second-order kinetic models. A plot of $\ln(C_0-C_t)$ versus times is used to describe the pseudo-first-order kinetic model as the following equations (14):

$$\ln(C_0 - C_t) = \ln(C_0) - k_1 t \qquad (14)$$

when k_1 is a pseudo-first-order rate constant obtained from the slope of the straight line.

The plot of $1/C_t$ versus times is described by the pseudo-second-order kinetic models as shown in the equation:

$$\frac{1}{C_t} = \frac{1}{C_0} + k_2 t \qquad (15)$$

2.7 Photocatalytic oxidation thermodynamics

The thermodynamic properties of the photocatalytic oxidation of $TiO_2/SrCO_3$ and $Ag.TiO_2/SrCO_3$ employed the Arrhenius equation. A plot between $\ln(k)$ and $\frac{1}{T}$ given a strength line and activation energy (E_a) can be found in the equation (16).

$$\ln(k) = \frac{-E_a}{RT} \qquad (16)$$

A plot between $\frac{\ln(k)}{T}$ and $\frac{1}{T}$ given a strength line and activation enthalpy ($\Delta H^\dagger$) can be calculated from slop and $\Delta S^\dagger$ can be found in the equation (17).

$$\frac{\ln(k)}{T} = \frac{\Delta H^\dagger}{RT} + \frac{\Delta S^\dagger}{R} \qquad (17)$$

The free energies ($\Delta G^\dagger$) at various temperatures can be calculated from eq. (18)

$$\Delta G^\dagger = \Delta H^\dagger - T\Delta S^\dagger \qquad (18)$$

3. Results and discussion

3.1 Characterization

The synthesized composite photocatalysts were obtained and characterized by scanning electron microscope (SEM). Figure 2 represents the SEM images for TiO_2, $SrCO_3$, and photocatalyst. It was found that the SEM images of $SrCO_3$ and photocatalyst are similar and TiO_2 is distributed on the surface of $SrCO_3$.

(A)

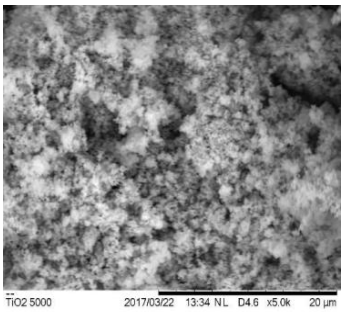

(B)

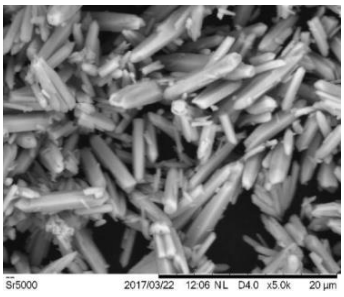

(C)

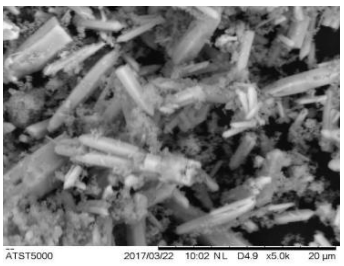

Figure 2 SEM images of TiO_2, $SrCO_3$, and TiO_2.$SrCO_3$ photocatalyst.

3.2 Effect of pH

The effects of various pH were investigated and the results are shown in Fig. 3. The experiment was conducted with an arsenic initial concentration of 1 ppm and 1 g of $TiO_2/SrTiO_3$. As shown in Fig. 4, the maximum removal of arsenic of 97% was observed in pH 1 and decreased gradually when pH was higher at 2, 3 and 5. As a result, the acidic condition, especially pH 1 led to the $TiO_2/SrTiO_3$ surface being mostly positive and attracted arsenic which possesses a negative charge to the surface via electrostatic force. This accelerates the conversion rate of arsenic [14].

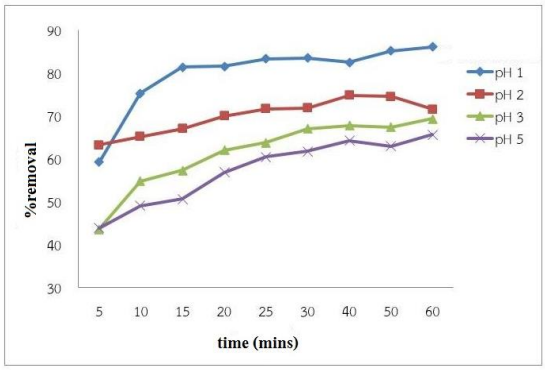

Figure 3 Effect of pH on the photocatalytic efficiency

3.3 Effects of initial arsenic concentration

The effect of different initial $NaAsO_2$ concentrations of its removal in pH 1 is shown in Fig. 3. It is shown that initial arsenic concentrations strongly affected its removal. The removal decreased as the initial concentration gradually increased from 0.5 to 50 ppm. When the amount of arsenic is small, the electron-hole separation would be archived. The photogenerated electrons efficiently transfer from the catalyst to adsorbed oxygen forming a larger number of reactive $O_2^{\bullet-}$ radical. The water molecules act as electron donors for hole regeneration then forming $OH^{\bullet}$. These radicals react with arsenic effectively and accelerate the oxidation of arsenic. However, a higher amount of arsenic leads to its deposition which could cover more on $TiO_2/SrCO_3$ surface and hinder the contact between $TiO_2/SrCO_3$ and arsenic which would increase diffuse distance and decrease the number of received photons. In addition, as the radical densities were equal in all solutions, a solution with a low concentration of arsenic with the same $OH^{\bullet}$ and $O_2^{\bullet-}$ formation rate

would have a higher conversion rate than a higher concentration of arsenic. The result is in agreement well with the previous experiment [15].

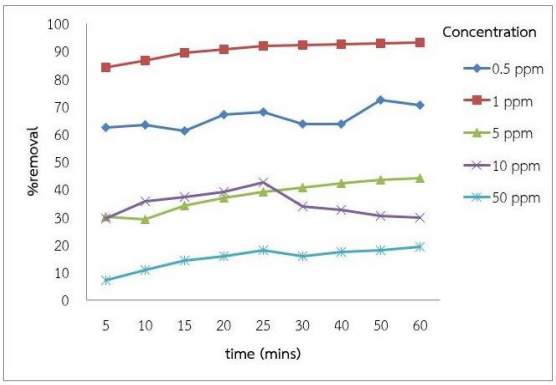

Figure 4 Effect of initial concentration of arsenic on photocatalytic efficiency

3.4 Effect of photocatalyst loading

The effects of different $TiO_2/SrCO_3$ loading on arsenic removal were investigated in Fig. 5. The concentration of arsenic is 1 ppm, pH 1. As shown in the Fig. 5, as the amount photocatalyst increased from 1 g to 1.5 g, the removal of arsenic is increased but the removal is decreased when the amount of photocatalyst is higher than 1.5 g. This may be due to the larger amount of photocatalyst obscuring the penetration of light leading to a decrease of photocatalytic oxidation of arsenic on photocatalyst surface.

3.5 Photocatalytic efficiency between $TiO_2/SrCO_3$ and $Ag.TiO_2/SrCO_3$

Based on the optimum condition for $TiO_2/SrCO_3$ including pH 1, initial concentration of arsenic 1 ppm, and catalyst loading 1 g, the photocatalytic efficiency of $Ag.TiO_2/SrCO_3$ was observed in the same condition. The photocatalytic efficiency of the two photocatalysts is shown in Fig. 6. As a result, the doping of silver accelerates the photocatalytic oxidation of arsenic from 92% to 96% which very high initial rate of removal (90%). The higher removal efficiency of $Ag.TiO_2/SrCO_3$ than $TiO_2/SrCO_3$ is due to the Ag atom capturing photogenerated electrons and transferring the electron effectively to oxygen molecule to form radical. In addition, the doping of the Ag atom can prohibit or decrease the electron-hole recombination which enhances the number of the photogenerated electrons in the conduction band of the photocatalyst.

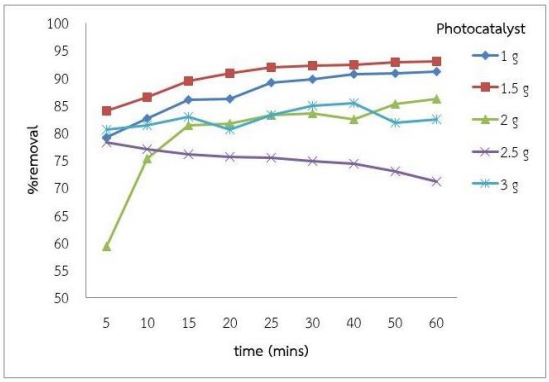

Figure 5 Effect of photocatalyst loading on photocatalytic

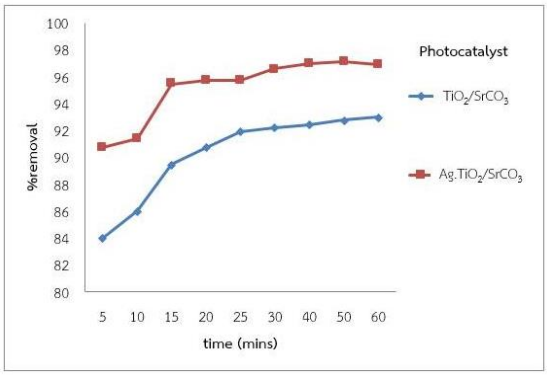

Figure 6 Photocatalytic oxidation of $TiO_2/SrCO_3$ and $Ag.TiO_2/SrCO_3$ and interval time

3.6 Kinetics of photocatalytic efficiency between $TiO_2/SrCO_3$ and $Ag.TiO_2/SrCO_3$

Kinetics of the photocatalytic oxidation of As^{3+} by $TiO_2/SrCO_3$ and $Ag.TiO_2/SrCO_3$ were observed. The kinetic data at various temperatures are shown in Table 1. Concentrations of As^{3+} in the test solution at the available time were determined from the standard concentration curve. Figure 7 represents a plot of ln ($[As^{3+}]_0/([As^{3+}]$) versus time and $1/[As^{3+}]$ versus time to follow the first-order and second-order kinetic reactions, respectively. Based on the R^2 of the linear plots, the kinetic of photocatalytic oxidation of $TiO_2/SrCO_3$ follows the second-order (R^2 0.9542) while of $Ag.TiO_2/SrCO_3$ follows the first-order (R^2 0.8675) model. It suggests that doping metal can change the kinetic of the photocatalyst.

Table 1 Rate constants of the kinetic models of photocatalytic oxidation of arsenic of $TiO_2/SrCO_3$ and $Ag.TiO_2/SrCO_3$

photocatalysts	T	Pseudo first order	Pseudo second order
	(K)	$k_1(m^{-1})$	$k_2(M^{-1}m^{-1})$
$TiO_2/SrCO_3$	33	3.50×10^{-2}	3.70×10^{-2}
	43	1.50×10^{-2}	6.90×10^{-4}
	53	8.00×10^{-3}	6.00×10^{-3}
$Ag.TiO_2/SrCO_3$	33	2.30×10^{-2}	1.30×10^{-2}
	43	8.00×10^{-3}	2.40×10^{-4}
	53	2.60×10^{-2}	1.60×10^{-5}

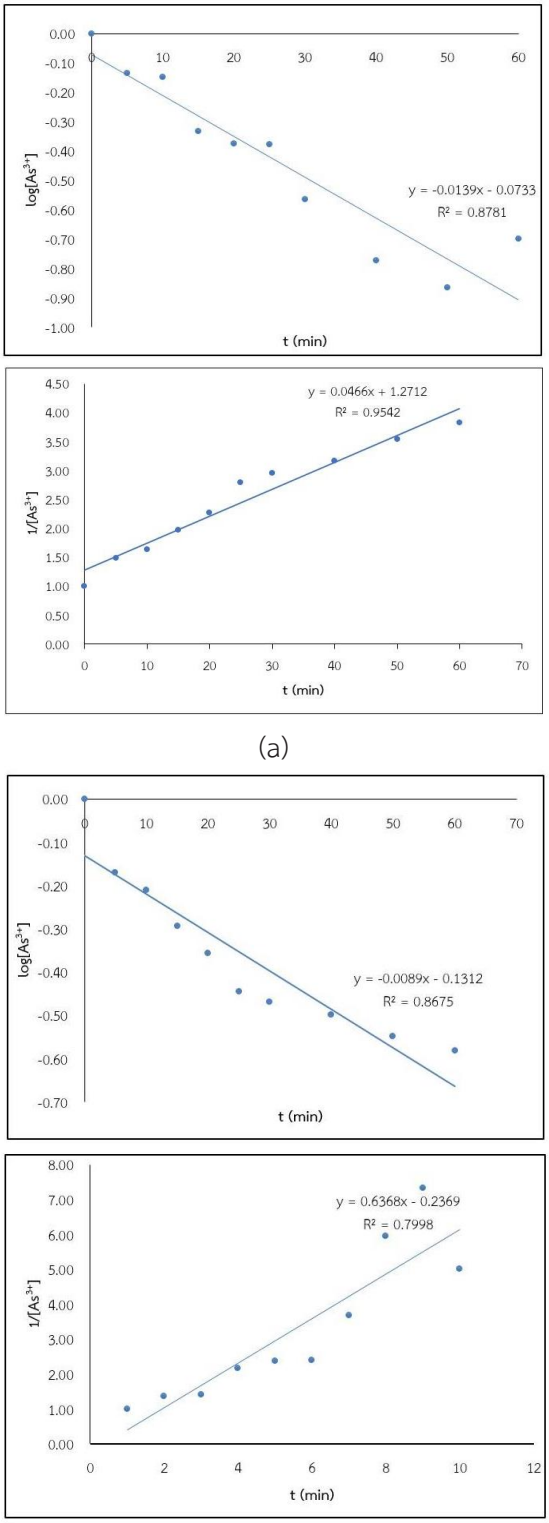

Figure 7 Linear plot of the first- and second-order kinetics of photocatalytic oxidation of arsenic by (a) $TiO_2/SrCO_3$ and (b) $Ag.TiO_2/SrCO_3$

3.7 Thermodynamics of photocatalytic efficiency between $TiO_2/SrCO_3$ and $Ag.TiO_2/SrCO_3$

A plot of ln(k) at various temperatures versus 1/T based on eq.16 of photocatalytic efficiency of the two photocatalysts is shown in Fig. 9. The corresponding activation energies are obtained from the slop. In addition, a plot of ln(k)/T at various temperatures versus 1/T based on eq.17 of photocatalytic efficiency of the two photocatalysts is also shown in Fig. 8. The corresponding activation enthalpy and entropy were obtained from the slope and y-intercept, respectively. The kinetic and thermodynamic data are tabulated in Table 2. Gibbs free energy of activation ($\Delta G^{\#}$), determines the rate at which a certain reaction will undergo at a given temperature, and as we see the reaction is possible under the conditions considered. The high values of $\Delta G^{\#}$ reveal that the formation of the activated complex is slow. Amount of binding energy; $\Delta H^{\#}$ is gained in the transition state relative to the ground state (including solvent effects). For a bimolecular reaction $\Delta S^{\#}$<<<0 J/mol.K^{-1}. The large negative value of $\Delta S^{\#}$ in this reaction suggests a considerable degree of charge separation in the activated complex. This results in an immobilization of a large number of solvent molecules, reflected in loss of entropy. The plots are based on eq. 16 and 17 are in agreement well with [16]. Doping of Ag clearly accelerates the catalytic activity of the $TiO_2/SrCO_3$ system.

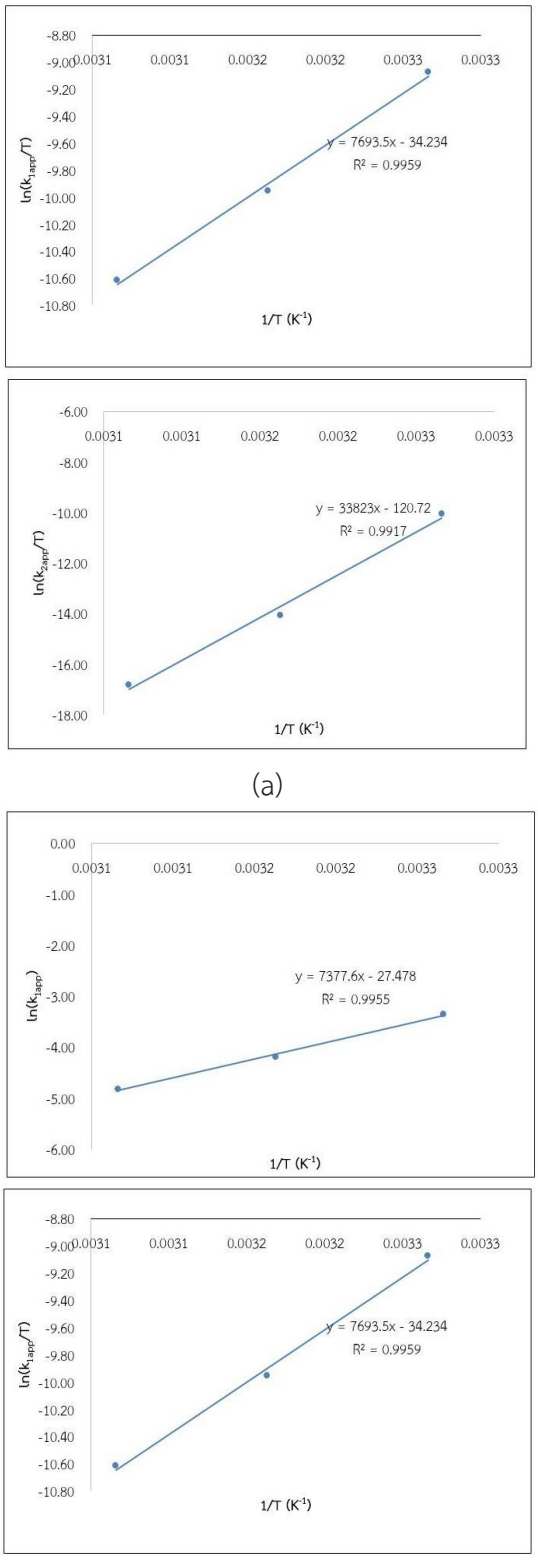

Figure 8 A plot of ln(k) at various temperatures versus 1/T and a plot of ln(k)/T at various temperatures versus 1/T

Table 2 Thermodynamic data of photocatalytic oxidation of arsenic by $TiO_2/SrCO_3$ and $Ag.TiO_2/SrCO_3$

$Ag.TiO_2/SrCO_3$				
Temp. (°C)	$\Delta E^{\#}$ (kJ/mol)	$\Delta H^{\#}$ (kJ/mol)	$\Delta S^{\#}$ (J/mol.K)	$\Delta G^{\#}$ (kJ/mol)
33				88.03
43	0.86	73.53	-287.33	90.91
53				93.79
$TiO_2/SrCO_3$				
Temp. (°C)	$\Delta E^{\#}$ (kJ/mol)	$\Delta H^{\#}$ (kJ/mol)	$\Delta S^{\#}$ (J/mol.K)	$\Delta G^{\#}$ (kJ/mol)
33				106.62
43	352.21	325.11	-347.19	110.09
53				113.56

4. Conclusion

Photocatalytic removal of As^{3+} from aqueous solution using synthesized $TiO_2/SrCO_3$ and $Ag.TiO_2/SrCO_3$ under solar light irradiation was studied. The effect of the initial concentration of As^{3+}, solution pH, photocatalyst loading, and temperature was taken into account. Maximum removal of As^{3+} was observed at pH 1, 1 ppm initial concentration of $As^{3+,}$ and 1 g of photocatalysts at ambient conditions. The removal efficiency of As^{3+} by $Ag.TiO_2/SrCO_3$ is higher than those of $TiO_2/SrCO_3$. The kinetics of both systems are different which photocatalytic kinetic of $TiO_2/SrCO_3$ followed the second-order while of $Ag.TiO_2/SrCO_3$ followed the first-order reaction.

5. Acknowledgement

This work was financially supported by The Faculty of Engineering, Khon Kaen campus to PH and JM through the undergraduate project development fund.

6. References

[1] Mahata, B. J., Gupta, S., and Giri, A.K. (2001) Genetic toxicology of a paradoxical human carcinogen, arsenic: *A review. Mutat. Res. Rev. Mutat. Res.* Vol.488, 171-194.

[2] Mandal, B.K., Suzuki, K.T., (2002) Arsenic round the world: A review. *Talanta*, vol.58, pp.201-235.

[3] USEPA, (2002), Arsenic and clarifications to compliance and new source contaminants monitoring: Final rule (66 FR 6976). *U.S. Environmental Protection Agency (USEPA),* USA., August 2002.

[4] Choong, T.S.Y., Chuah, T.G., Robiah, Y., Koay, F.L.G., and Azni, I. (2007) Arsenic toxicity, health harzards and removal techniques from water: An overview, *Desalination*, vol.217, pp.139-166.

[5] Hering, J.G., Chen, P.Y., Wilkie J.A., and Elimelech, M. (1997) Arsenic removal from drinking water during coagulation. *J. Environ. Eng.* vol.123, pp.800-807.

[6] Waypa, J.J., Elimelech, M., and Hering, J.G. (1997) Arsenic removal bu RO and NF membrane, *J. Am. Water Works Assoc.* vol.89, pp.102-114.

[7] Wahabet, R.I., Hwang, H., Kim, Y.-S. (2011) Non-hydrolytic synthesis and photo-catalytic studies of ZnO nanoparticles, *Chem. Eng. J.* vol.175, pp.450–457.

[8] Byrappa, K., Subramani, A.K., Ananda, S., Rai, K.M.L., Dinesh, R., and Yoshimura, M. (2006) Photocatalytic degradation of rhodamine B dye using hydrothermally synthesized ZnO, *Bull. Mat. Sci.,* vol.29(5), pp.433–438.

[9] Soltaninezhad M., and Aminifar, A. (2011) Study nanostructures of semiconductor zinc oxide (ZnO) as a photocatalyst for the degradation of organic pollutants, *Int. J. Nano. Dimens.,* vol.2(2), pp.137–145,

[10] Sathishkumar, P., Pugazhenthiran, N., Mangalaraja, R.V., Asiri, A.M., and Anandan, S. (2013) ZnO supported CoFe2O4 nanophotocatalysts for the mineralization of Direct Blue 71 in aqueous environments, *J. Haz. Mat.* Vol.252-253, pp.171–179.

[11] Awual, M.R., Urata, S., Jyo, A., Tamadam, M., and Katakai, A. (2008) Arsenate removal from water by a weak-base anion exchange fibrous adsorbent. *Water Res.* vol.42, pp. 689-696.

[12] Rajabi, H. R., Khani, O., Shamsipur, M., and Vatanpour, V. (2013) High performance pure and Fe ion doped ZnS quantum dots as green nanophotocatalysts for the removal of malachite green under UV-light irradiation, *J. Haz. Mat.* vol.250-251, pp.370–378.

[13] Karimi, L., Zohoori, S., and Yazdanshenas, M.E., (2014) Photocatalytic degradation of azo dyes in aqueous solutions under UV irradiation using nano-strontium titanate as the nanophotocatalyst, *J. Saudi. Chem. Soc.* vol.18(5) pp.581–588.

[14] Kummung, S., Wongwilas, S., Somseemee, O., Sang-aroon W. (2014), Photocatalytic reduction of Cr(VI) in aqueous solution by silver doped zinc oxide under ultraviolet light irradiation, *RMUTI J*, vol.6(2), pp.1-14.

[15] KalpeshIsai, A.I., and Shrivastava, V. (2019) Photocatalytic degradation of methylene blue using ZnO and 2%Fe–ZnO semiconductor nanomaterials synthesized by sol–gel method: a comparative study, *SN Applied Sciences*, 1(10) pp.1247-1257.

[16] Tinsay, M., and Siraj, K. (2011). Kinetics and Mechanism of Oxidation of Glycolic Acid by Hexamethylenetetramine-Bromine in Glacial Acetic Acid Medium. *European Journal of Scientific Research.* 49. 49-60.